however, grew much slower than that in the presence of heparin. The sizes of the aggregated particles were measured by the dynamic light scattering method; after 20 min, the aggregations grew into large particles with mean hydrodynamic radiuses of 206.8 ± 130.6 and 16.30 ± 8.97 nm in the presence and absence of heparin, respectively. These aggregations were still soluble in the aqueous solution at that time, but precipitated within 60 h. In contrast, the labeled R4 peptide did not aggregate under the same condition (Fig. 2b), as reported by Mizushima *et al.* (2006). These results indicate that the R3 peptide intrinsically has a high propensity to aggregate. Heparin was not necessary for the R3 peptide to aggregate, but it enhanced aggregation of the R3 peptide.

Saturation point. What is the minimum concentration (saturation point) for the R3 peptide to aggregate? In general, proteins have higher aggregation propensities at lower saturation points. Is this general property true for the R3 peptide? To answer this question, we investigated aggregation of the R3 peptide at three different concentrations, 1, 5 and 10 μM, to elucidate its concentration-dependence in aggregation, in the absence of any inducer. Figure 2c shows that 5 and 10 μM of the peptide formed aggregates, whereas 1 μM of the peptide did not. These results indicate that the saturation point of the R3 peptide is between 1 and 5 μM in the absence of heparin. This value is similar to the saturation point for the intact tau protein observed in the presence of heparin (Carlson *et al.*, 2007). This, however, seems quite high in contrast with the α-amyloid (1–40) peptide, which aggregates at 40 nM under a specific condition (Ding *et al.*, 2012). Thus, the tau protein may be rather soluble among proteins forming amyloid-like fibers.

Oxidation. The tau protein isoforms have, at most, two cysteine residues. For example, the N2R4 isoform (441 amino acid residues) contains Cys291 and Cys322. Both cysteine residues are located in the MBD, Cys291 in the R2 region, and Cys322 in the R3 region. These cysteine residues formed intramolecular and intermolecular disulfide bonds and accelerated the aggregation of tau peptides (Sugino *et al.*, 2009). In the present study, only one cysteine residue, Cys322 (Cys17 in the R3 peptide's sequence), was included in the R3 peptide, suggesting that it was able to dimerize the peptide under oxidative conditions. Thus, we investigated how the oxidation of Cys17 affected the aggregation of the R3 peptide. Figure 2d shows that the R3 peptide aggregated much faster under the oxidative condition than under the reductive condition, suggesting that dimerization of the R3 peptide accelerates the aggregation. According to Sugino *et al.* (2009), two types of tau peptides, 4RMDB (R1–R2–R3–R4) and 3RMDB (R1–R3–R4), formed homodimers, with an intramolecular and intermolecular disulfide bond, respectively. After dimerization, the peptides assemble into large aggregations, depending on their sequences. The R3 peptide also aggregated under the oxidative condition, and the aggregation rate was almost the same as that of the rate of 3RMDB. Thus, the mechanism of aggregation of the R3 peptide was expected to be the same as that of 3RMDB, although they did not specifically mention it (Sugino *et al.*, 2009). The disulfide bonds, however, were not essential for the aggregation of tau peptides, including R3, 3RMDB and 4RMBD. These tau peptides aggregated, even under the reductive condition (Fig. 2d) (Sugino *et al.*, 2009), suggesting that the aggregation mechanism under the reductive condition was different from the mechanism under the oxidative condition.

Salt effect. As shown above, heparin accelerated aggregation of the R3 peptide (Fig. 2a), suggesting that the aggregation of the peptide was driven mainly by hydrophilic interactions. Here, we measured the aggregation of the R3 peptide under various salt concentrations in the presence of the reductant to elucidate the charge effect on the aggregation. Figure 2e shows that the aggregation of the R3 peptide decreased when the salt concentration increased. The R3 peptide did not aggregate in the presence of 400 mM of sodium chloride. This result also indicated that the hydrophilic interactions affect the aggregation of the R3 peptide considerably.

pH dependency. We next investigated the type of hydrophilic amino acid residues responsible for aggregation of the R3 peptide. The R3 peptide includes eight hydrophilic residues, one aspartic acid residue, two histidine residues, four lysine residues and one tyrosine residue. Thus, we measured the aggregation of the R3 peptide at five different pHs, 4.5, 5.9, 6.9, 8.0 and 9.4, in the presence of reductant. The electrostatic interaction of the R3 peptide almost vanished at pH 9.4, because the isoelectric point of the R3 peptide is theoretically 9.98. This suggests that the hydrophobic effects were greatest at pH 9.4. In contrast, lower the pH becomes, more positive the net charge of the R3 peptide becomes. This suggests that the hydrophilic effects become the largest at pH 5.9. At the mid-range pHs, both the hydrophilic and hydrophobic effects were medium, but distribution of the local charge of the R3 peptide was dependent on the pH. We found that aggregation of the R3 peptide was at the minimum and maximum levels at pH 6.9 and 8.0, respectively (Fig. 2f), suggesting that the distribution of the local charge was more important for aggregation of the R3 peptide than the net charge of the peptide. Furthermore, the transition to aggregation of the R3 peptide occurred between pH 6.9 and 8.0, suggesting that distribution of the local charge of the peptide changed between pH 6.9 and 8.0. One of the candidate mechanisms for changing the charge is deprotonation of the histidine residue. The R3 peptide contains two histidine residues, His24 and His25. The local positive charge around the histidine residues might be related to aggregation of the R3 peptide.

In summary, the R3 peptide aggregated even in the absence of inducer, and the aggregation was driven by hydrophilic interaction. The deprotonation of histidine seemed to affect aggregation of the peptide.

Aggregation inhibition by FKBP12

The R3 peptide contains two proline residues, Pro7 and Pro27. The proline residues are not the target for Pin1 but are the targets for FKBP12, because Lys6 and Lys26 precede the proline residues (Yaffe, 1997). In order to elucidate the aggregation inhibitory activity of FKBP12, we measured aggregation of the R3 peptide in various concentrations of FKBP12 by change of fluorescence intensity of fluorescein. Figure 3a shows that R3 peptide aggregation decreased when the concentration of FKBP12 increased. No peptide aggregation was detected in the presence of 20 μM of FKBP12. This result clearly indicated that FKBP12 prevents the R3 peptide from aggregating. We calculated that 50% inhibitory concentration (IC_{50}) of FKBP12 under the conditions was 3 μM (Fig. 3b).

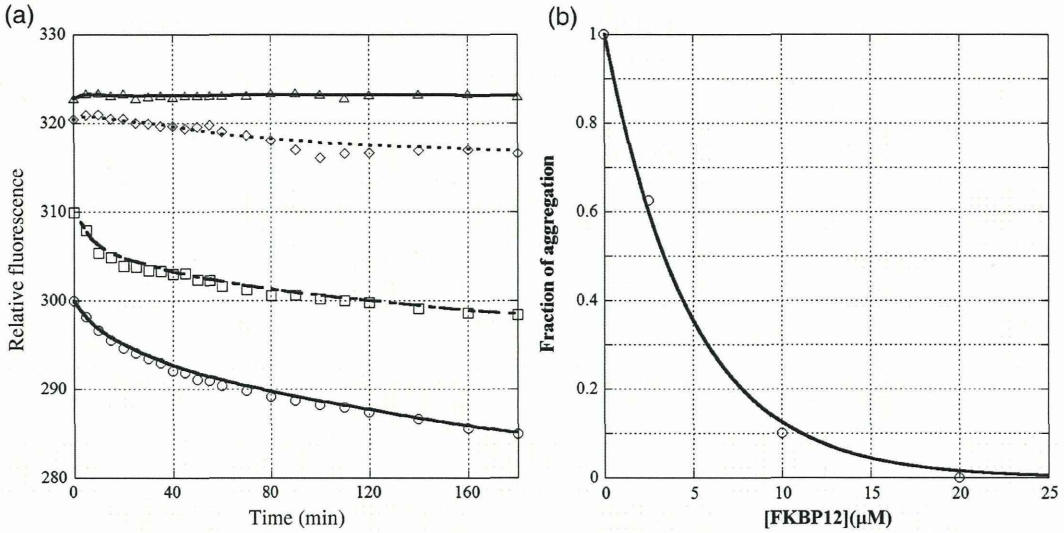

Fig. 3. (**a**) Aggregation of the R3 peptides in the presence of FKBP12. The aggregation of 5 μM of the R3 peptide was monitored in the presence of 0 (empty circle), 2.5 (empty square), 10 (empty rhombus) or 20 (empty triangle) μM FKBP12 at pH 8.0 and 25°C with the relative fluorescence of fluorescein. The reaction started by diluting 0.5-mM stock solution of the peptide 100 times. The reaction mixture also contained 50 mM sodium phosphate and 10 mM TCEP. Curve fitting was performed by applying a Stineman interpolating function to the data on KaleidaGraph (Hukinks). (**b**) The normalized amount of aggregation in the presence of FKBP12. The normalized amount of aggregation was calculated by dividing the decrease in fluorescence during the first 180 min by the decrease in the absence of FKBP12. Curve fitting was based on the two-state transition theory. The 50% inhibitory concentration (IC_{50}) of FKBP12 was calculated at 3 μM on the basis of this graph.

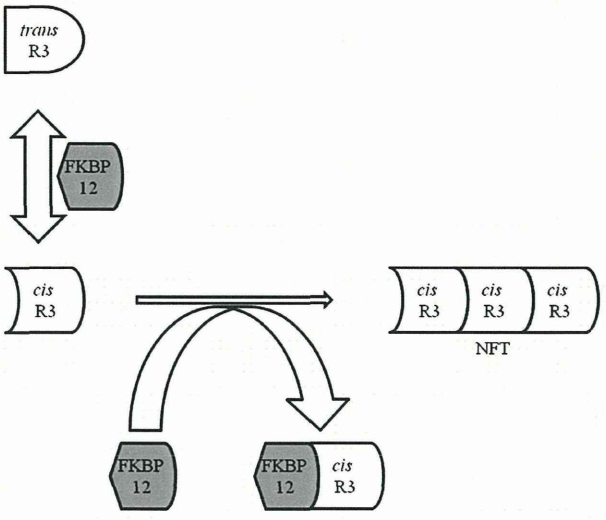

Scheme 1. The inhibitory mechanism of R3 peptide aggregation by simple binding of FKBP12. In this scheme, only the *cis*-isomer of the R3 peptide can aggregate, to which FKBP12 specifically and tightly binds. FKBP12 catalyzes isomerization of Xaa-Pro motifs of the R3 peptide only in the monomeric state. Association between FKBP12 and the *cis*-isomer is much faster than self-association of the *cis*-isomer because the concentration of the *cis*-isomer is very low. Therefore, FKBP12 intercepts the *cis*-isomer during its aggregation.

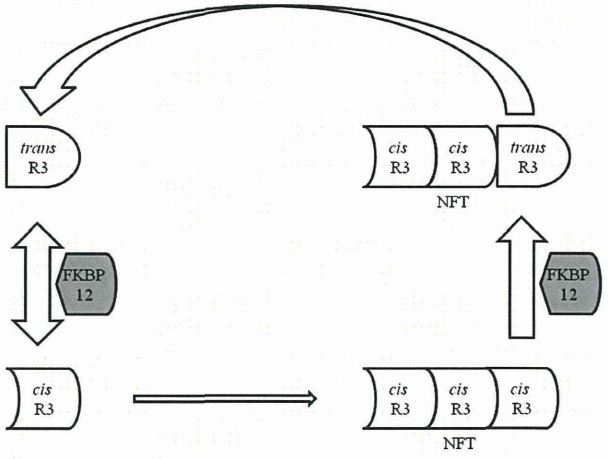

Scheme 2. The inhibitory mechanism of R3 peptide aggregation by PPIase activity of FKBP12. In this scheme, only the *cis*-isomer of the R3 peptide can aggregate, and FKBP12 does not tightly bind to either isomer. FKBP12 catalyzes isomerization of Xaa-Pro motifs of the R3 peptide in both the monomeric and aggregative state. Once the *cis*-isomer is converted into the *trans*-isomer in the aggregative state, the *trans*-isomer is quickly released from the aggregation because the *trans*-isomer cannot aggregate.

There are two possible explanations for the mechanism of how FKBP12 prevents the R3 peptide from aggregating (Schemes 1 and 2). One is that FKBP12 sequesters the R3 peptide: (i) FKBP12 tightly binds to the R3 peptide, (ii) the effective concentration of the R3 peptide decreases to less than its saturation point and (iii) FKBP12 also interacts with oligomers of the R3 peptide at the early stage of aggregation, leading to dissociation of the peptide (Scheme 1). The other possible explanation is that FKBP12 catalyzes isomerization from the higher aggregation-prone isomer to the lower one: (i) FKBP12 binds more tightly to the higher aggregation-prone isomer of the R3 peptide than to the lower one, and (ii) FKBP12 catalyzes isomerization from the higher aggregation-prone isomer to the lower one as well as Pin1 and (iii) FKBP12 also functions for oligomers of the R3 peptide at the early stage of aggregation, leading to dissociation of the peptide (Scheme 2). Both schemes have the association of FKBP12 with the R3 peptide in common. However, they are

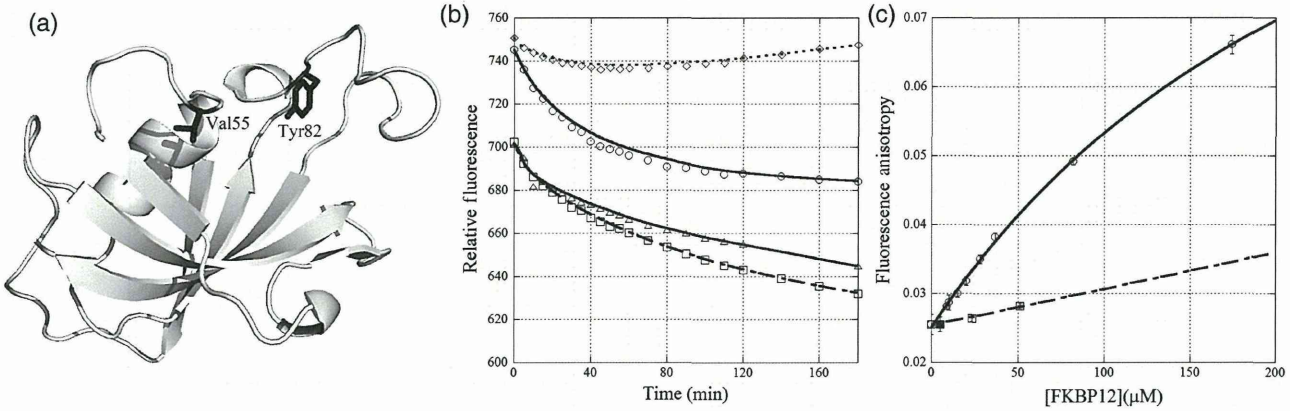

Fig. 4. (**a**) The positions of mutations on the tertiary structure of FKBP12. The two residues are drawn with a stick model. (**b**) Aggregation of 5 μM of the R3 peptides in the presence of 5 μM wild-type FKBP12 (empty circle), 5 μM FKBP12/Tyr82Lys (empty square) and 5 μM FKBP12/Val55Arg (empty rhombus), and in the absence of FKBP12 (empty triangle). The other conditions are the same as described in Fig. 3. Curve fitting was performed by applying a Stineman interpolating function to the data on KaleidaGraph (Hukinks). (**c**) Fluorescence depolarization of fluorescein attached to the R3 peptide for titration of wild-type FKBP12 (empty circle), FKBP12/Tyr82Lys (empty square) and FKBP12/Val55Arg (filled square). The concentration of R3 peptide needed to prevent aggregation was 1 μM. Curve fitting was based on the two-state transition theory. The dissociation constant (K_d) for wild-type FKBP12 was calculated at 271 μM. The K_d values for the mutant proteins could not be determined because of the very weak interaction between the peptide and the mutant proteins.

different in the catalytic reaction of FKBP12. FKBP12 only sequesters the peptide in the former scheme, while it catalyzes the isomerization of Xaa-Pro bonds of the peptide in the latter scheme.

To determine which scheme is applicable to the function of FKBP12, we introduced two types of mutations into FKBP12; one mutation increased the PPIase activity, and the other mutation decreased the activity. A Val55 → Arg mutation (FKBP12/Val55Arg) increased PPIase activity by a factor of 11, while a Tyr82 → Lys mutation (FKBP12/Tyr82Lys) decreased the activity by a factor of 7 (Fig. 4a) (Ikura and Ito, 2007). In order to elucidate the effect of PPIase activity, we measured the aggregation of 5 μM of the R3 peptide in the presence of 5 μM of each of these mutant proteins by change in fluorescence intensity of fluorescein. Moreover, in order to elucidate how the mutations affect the association between FKBP12 and the R3 peptide, we measured the affinities of the proteins to the R3 peptide by the fluorescence depolarization method. In this affinity study, concentration of the R3 peptide was decreased to 1 μM because the R3 peptide did not aggregate at this concentration (Fig. 2c). As the results indicated, the R3 peptide did not aggregate in the presence of FKBP12/Val55Arg, while FKBP12/Tyr82Lys did not inhibit the aggregation (Fig. 4b). In the presence of FKBP12/Val55Arg, the R3 peptide aggregated transiently at first, then gradually dissociated and finally, the peptide was completely restored from the aggregation. The apparent dissociation constant (K_d) for wild-type FKBP12 was calculated as 271 μM, whereas the K_ds for each of the two mutants was much >271 μM (Fig. 4c). These affinities were too low for K_d calculation by the fluorescence depolarization method. These results indicated that higher the PPIase activity of FKBP12, higher its aggregation inhibitory activity. The results also indicated that the aggregation inhibitory activity of FKBP12 was independent of the affinity between FKBP12 and the R3 peptide. Therefore, the aggregation inhibitory activity of FKBP12 depended only on the PPIase activity of FKBP12, as represented by Scheme 2.

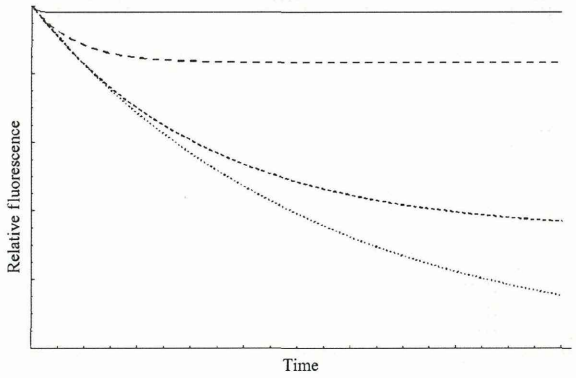

Fig. 5. Theoretical analysis of the aggregation of the R3 peptide in the presence of FKBP12. Each curve was calculated by numerically solving the differential equations derived from Scheme 2. The solid and dotted lines indicate the highest and lowest concentrations of FKBP12, respectively. Two dashed lines represent the mid-level concentration of FKBP12. This figure reflects Fig. 3 as well, indicating that Scheme 2 is a good descriptor of the function of FKBP12.

Discussions

Mechanism of FKBP12 inhibition of R3 peptide aggregation

As shown in Fig. 3a, 20 μM of FKBP12 completely inhibited aggregation of the R3 peptide. Mutational studies on FKBP12 showed that the aggregation inhibitory activity of FKBP12 is attributable mainly to its PPIase activity (Fig. 4b and c). Furthermore, FKBP12 not only acted on the R3 peptide in the monomeric state but also in the aggregative state (Fig. 4a). This restoration of the R3 peptide from aggregate to monomer suggests that the R3 peptide aggregation formed at the early stage does not strongly resist the attack by FKBP12. These features of the aggregation of the R3 peptide in the presence of FKBP12 are well described in Scheme 2. On the other hand, the mutational studies showed that the aggregation inhibitory mechanism of FKBP12 was inconsistent with Scheme 1, because the mutation Val55 → Arg weakened the association

between FKBP12 and the peptide, but raised the aggregation inhibitory activity (Fig. 4b and c). Here, we theoretically examined how Scheme 2 reproduced the experimental results. In simulating the inhibition of R3 peptide aggregation by FKBP12 in Scheme 2, we simplified the reaction so that (i) only the *cis*-isomer of the Xaa-Pro motif aggregated irreversibly, (ii) FKBP12 accelerated the isomerization between *cis*- and *trans*-isomers in monomeric and aggregative states and (iii) only the *trans*-isomer in the aggregative state quickly dissociated from the aggregation. As a result, the acceleration of isomerization decreased the amount of aggregation of the R3 peptide (Fig. 5), indicating that Scheme 2 describes the experimental results, in which FKBP12 restored the R3 peptide from the aggregation. Although no structural information is available to explain the difference between the *cis*- and *trans*-isomers, we can interpret this issue on the basis of pH dependency of the aggregation (Fig. 2f). Aggregation of the R3 peptide was sensitive to the distribution of local charge. The *cis*- and *trans*-isomers are probably different from each other in the distribution of local charge. Therefore, the *cis*-isomer is much aggregative than the *trans*-isomer, as reported for the aggregation propensity of the pThr231-Pro232 motif (Nakamura *et al.*, 2012).

In 2001, von Bergen *et al.* pointed out that Pro312 was important for aggregation propensity of the R3 peptide (von Bergen *et al.*, 2001). They reported that a deletion mutant of a short R3 peptide (Val306-Lys317), which lacked only Pro312, showed a pronounced shift to β-structure and enhanced the aggregation, indicating that the aggregation propensity of the R3 peptide correlated with the β-structure content for residues around the Val306-Lys311 motif, and Pro312 in the intact sequence broke elongation of β-structure by its restricted conformation. This means that Pro312 suppresses aggregation of the R3 peptide. Although they did not investigate the isomerization of Pro312, this suppressive effect should be brought about by the *trans*-isomer because it is in majority. The *cis*-isomer might have higher β-structure content for the R3 peptide than the *trans*-isomer. Therefore, isomerization of Pro312 presumably attributes to the aggregation propensity of the R3 peptide.

In vivo *function of FKBP12*

FKBP12 was first discovered as the receptor for an immunosuppressor in the immune system (Harding *et al.*, 1989; Siekierka *et al.*, 1989). It was later revealed that FKBP12 had multiple functions in cells. FKBP12 interacts with signal transduction proteins such as the type-1 transforming growth factor receptor (Chen *et al.*, 1997), and with multiple intracellular calcium release channels, such as the tetrameric skeletal muscle ryanodine receptor (Gaburjakova *et al.*, 2001). FKBP12 is also abundantly expressed in the brain and accumulates in NFT (Sugata *et al.*, 2009). However, whether or not FKBP12 is concerned with the aggregation process of tau protein was still unclear. In this study, we clearly demonstrated that FKBP12 prevented the R3 peptide from aggregating *in vitro*. Although a short fragment of tau protein, the R3 region was essential for tau protein to aggregate (Perez *et al.*, 2007). Therefore, it is expected that FKBP12 prevents tau protein aggregation by interacting with the R3 region of tau protein *in vivo*, as it acts upon the R3 peptide *in vitro*. In its *in vitro* aggregation inhibitory activity, FKBP12 catalyzed the isomerization both of monomeric and aggregative states, suggesting that such isomerization catalysis is also essential for its *in vivo* aggregation inhibitory activity.

PPIase versus NFT

At least four PPIases, Pin1, FKBP12, FKBP51 and FKBP52, are estimated to be responsible for stabilizing and destabilizing the tau protein *in vivo* (Cao and Konsolaki, 2011; Nakamura *et al.*, 2012). Pin1 interacts with the pSer/Thr-Pro motifs in the tau protein and isomerizes the higher aggregative *cis*-isomer to the low aggregative *trans*-isomer. The functions of FKBP51 and FKBP52 are related to association and dissociation between the tau protein and two types of tubulins. However, whether or not the PPIase activities of both FKBPs are concerned with the function is unknown, because they consist of several functional domains. On the other hand, this study suggested that PPIase activity of FKBP12 was essential in preventing tau protein aggregation. Thus, many PPIases and their PPIase activities regulate the tau protein. Such a feature of the tau protein might be related to one of its structural properties, in which it is intrinsically disordered (Skrabana *et al.*, 2006).

Acknowledgements

We thank Professor Nobuhiro Takahashi (Tokyo University of Agriculture and Technology) for providing the cloned gene of human FKBP12.

Funding

This work was supported by Grants-in-Aid for Scientific Research (No 22113504) from the Ministry of Education, Culture, Sports, Science and Technology of Japan.

References

Bramblett,G.T., Goedert,M., Jakes,R., Merrick,S.E., Trojanowski,J.Q. and Lee,V.M. (1993) *Neuron*, **10**, 1089–1099. First published on 1993/06/01.

Brion,J.P., Smith,C., Couck,A.M., Gallo,J.M. and Anderton,B.H. (1993) *J. Neurochem.*, **61**, 2071–2080. First published on 1993/12/01.

Cao,W. and Konsolaki,M. (2011) *J. Biosci.*, **36**, 493–498. First published on 2011/07/30.

Carlson,S.W., Branden,M., Voss,K., Sun,Q., Rankin,C.A. and Gamblin,T.C. (2007) *Biochemistry*, **46**, 8838–8849. First published on 2007/07/05, doi: 10.1021/bi700403a.

Chambraud,B., Sardin,E., Giustiniani,J., Dounane,O., Schumacher,M., Goedert,M. and Baulieu,E.E. (2010) *Proc. Natl Acad. Sci. USA*, **107**, 2658–2663. First published on 2010/02/06, doi: 10.1073/pnas.0914957107.

Chen,Y.G., Liu,F. and Massague,J. (1997) *EMBO J.*, **16**, 3866–3876. First published on 1997/07/01, doi: 10.1093/emboj/16.13.3866.

Ding,H., Schauerte,J.A., Steel,D.G. and Gafni,A. (2012) *Biophys. J.*, **103**, 1500–1509. First published on 2012/10/16, doi: 10.1016/j.bpj.2012.08.051.

Gaburjakova,M., Gaburjakova,J., Reiken,S., Huang,F., Marx,S.O., Rosemblit,N. and Marks,A.R. (2001) *J. Biol. Chem.*, **276**, 16931–16935. First published on 2001/03/30, doi: 10.1074/jbc.M100856200.

Goedert,M., Wischik,C.M., Crowther,R.A., Walker,J.E. and Klug,A. (1988) *Proc. Natl Acad. Sci. USA*, **85**, 4051–4055. First published on 1988/06/01.

Goedert,M., Jakes,R., Crowther,R.A., Six,J., Lubke,U., Vandermeeren,M., Cras,P., Trojanowski,J.Q. and Lee,V.M. (1993) *Proc. Natl Acad. Sci. USA*, **90**, 5066–5070. First published on 1993/06/01.

Hamdane,M., Smet,C., Sambo,A.V., *et al.* (2002) *J. Mol. Neurosci.*, **19**, 275–287. First published on 2003/01/24, doi: 10.1385/JMN:19:3:275.

Hamdane,M., Dourlen,P., Bretteville,A., *et al.* (2006) *Mol. Cell. Neurosci.*, **32**, 155–160. First published on 2006/05/16, doi: 10.1016/j.mcn.2006.03.006.

Harding,M.W., Galat,A., Uehling,D.E. and Schreiber,S.L. (1989) *Nature*, **341**, 758–760. First published on 1989/10/26, doi: 10.1038/341758a0.

Ikura,T. and Ito,N. (2007) *Protein Sci.*, **16**, 2618–2625. First published on 2007/11/22, doi: 10.1110/ps.073203707.

Jinwal,U.K., Koren,J., III, Borysov,S.I., *et al.* (2010) *J. Neurosci.*, **30**, 591–599. First published on 2010/01/15, doi: 10.1523/JNEUROSCI.4815-09.2010.

Kopke,E., Tung,Y.C., Shaikh,S., Alonso,A.C., Iqbal,K. and Grundke-Iqbal,I. (1993) *J. Biol. Chem.*, **268**, 24374–24384. First published on 1993/11/15.
Lakowicz,J.R. (1983) *Principles of Fluorescence Spectroscopy*. Plenum Press, New York.
Landrieu,I., Leroy,A., Smet-Nocca,C., *et al.* (2010) *Biochem. Soc. Trans.*, **38**, 1006–1011. First published on 2010/07/28, doi: 10.1042/BST0381006.
Lindwall,G. and Cole,R.D. (1984) *J. Biol. Chem.*, **259**, 12241–12245. First published on 1984/10/10.
Liu,F., Li,B., Tung,E.J., Grundke-Iqbal,I., Iqbal,K. and Gong,C.X. (2007) *Eur. J. Neurosci.*, **26**, 3429–3436. First published on 2007/12/07, doi: 10.1111/j.1460-9568.2007.05955.x.
Lu,P.J., Wulf,G., Zhou,X.Z., Davies,P. and Lu,K.P. (1999) *Nature*, **399**, 784–788. First published on 1999/07/03, doi: 10.1038/21650.
Mizushima,F., Minoura,K., Tomoo,K., Sumida,M., Taniguchi,T. and Ishida,T. (2006) *Biochem. Biophys. Res. Commun.*, **343**, 712–718. First published on 2006/03/28, doi: 10.1016/j.bbrc.2006.02.185.
Morishima-Kawashima,M., Hasegawa,M., Takio,K., Suzuki,M., Yoshida,H., Watanabe,A., Titani,K. and Ihara,Y. (1995) *Neurobiol. Aging*, **16**, 365–371. discussion 371–380. First published on 1995/05/01.
Nakamura,K., Greenwood,A., Binder,L., Bigio,E.H., Denial,S., Nicholson,L., Zhou,X.Z. and Lu,K.P. (2012) *Cell*, **149**, 232–244. First published on 2012/04/03, doi: 10.1016/j.cell.2012.02.016.
Ogawa,Y., Nonaka,Y., Goto,T., *et al.* (2010) *Nat. Commun.*, **1**, 86. First published on 2010/10/29, doi: 10.1038/ncomms1090.
Perez,M., Arrasate,M., Montejo De Garcini,E., Munoz,V. and Avila,J. (2001) *Biochemistry*, **40**, 5983–5991. First published on 2001/05/16.
Perez,M., Santa-Maria,I., Tortosa,E., Cuadros,R., Del Valle,M., Hernandez,F., Moreno,F.J. and Avila,J. (2007) *J. Neurochem.*, **103**, 1447–1460. First published on 2007/08/08, doi: 10.1111/j.1471-4159.2007.04834.x.
Ramakrishnan,P., Dickson,D.W. and Davies,P. (2003) *Neurobiol. Dis.*, **14**, 251–264. First published on 2003/10/24.
Siekierka,J.J., Hung,S.H., Poe,M., Lin,C.S. and Sigal,N.H. (1989) *Nature*, **341**, 755–757. First published on 1989/10/26, doi: 10.1038/341755a0.
Skrabana,R., Skrabanova,M., Csokova,N., Sevcik,J. and Novak,M. (2006) *Bratisl. Lek. Listy*, **107**, 354–358. First published on 2007/02/01.
Smet,C., Sambo,A.V., Wieruszeski,J.M., Leroy,A., Landrieu,I., Buee,L. and Lippens,G. (2004) *Biochemistry*, **43**, 2032–2040. First published on 2004/02/18, doi: 10.1021/bi035479x.
Sugata,H., Matsuo,K., Nakagawa,T., Takahashi,M., Mukai,H., Ono,Y., Maeda,K., Akiyama,H. and Kawamata,T. (2009) *Neurosci. Lett.*, **459**, 96–99. First published on 2009/05/06, doi: 10.1016/j.neulet.2009.04.062.
Sugino,E., Nishiura,C., Minoura,K., In,Y., Sumida,M., Taniguchi,T., Tomoo,K. and Ishida,T. (2009) *Biochem. Biophys. Res. Commun.*, **385**, 236–240. First published on 2009/05/20, doi: 10.1016/j.bbrc.2009.05.047.
von Bergen,M., Barghorn,S., Li,L., Marx,A., Biernat,J., Mandelkow,E.M. and Mandelkow,E. (2001) *J. Biol. Chem.*, **276**, 48165–48174. First published on 2001/10/19, doi: 10.1074/jbc.M105196200.
Weber,G. (1953) *Adv. Protein Chem.*, **8**, 415–459. First published on 1953/01/01.
Weingarten,M.D., Lockwood,A.H., Hwo,S.Y. and Kirschner,M.W. (1975) *Proc. Natl Acad. Sci. USA*, **72**, 1858–1862. First published on 1975/05/01.
Yaffe,M.B. (1997) *Science*, **278**, 1957–1960. First published on, doi: 10.1126/science.278.5345.1957.
Yoshida,H. and Ihara,Y. (1993) *J. Neurochem.*, **61**, 1183–1186. First published on 1993/09/01.
Zhou,X.Z., Kops,O., Werner,A., *et al.* (2000) *Mol. Cell*, **6**, 873–883. First published on 2000/11/25.
Zhou,L.X., Zeng,Z.Y., Du,J.T., Zhao,Y.F. and Li,Y.M. (2006) *Biochem. Biophys. Res. Commun.*, **348**, 637–642. First published on 2006/08/08, doi: 10.1016/j.bbrc.2006.07.099.

OPEN ACCESS Freely available online

PLOS ONE

High Resolution Crystal Structure of the Grb2 SH2 Domain with a Phosphopeptide Derived from CD28

Kunitake Higo[1], Teikichi Ikura[2], Masayuki Oda[3], Hisayuki Morii[4], Jun Takahashi[1], Ryo Abe[1], Nobutoshi Ito[2]*

1 Research Institute for Biomedical Sciences, Tokyo University of Science, Noda-shi, Chiba, Japan, **2** Medical Research Institute, Tokyo Medical and Dental University, Bunkyo-ku, Tokyo, Japan, **3** Graduate School of Life and Environmental Sciences, Kyoto Prefectural University, Sakyo-ku, Kyoto-shi, Kyoto, Japan, **4** Biomedical Research Institute, National Institute of Advanced Industrial Science and Technology, Tsukuba-shi, Ibaraki, Japan

Abstract

Src homology 2 (SH2) domains play a critical role in cellular signal transduction. They bind to peptides containing phosphotyrosine (pY) with various specificities that depend on the flanking amino-acid residues. The SH2 domain of growth-factor receptor-bound protein 2 (Grb2) specifically recognizes pY-X-N-X, whereas the SH2 domains in phosphatidylinositol 3-kinase (PI3K) recognize pY-X-X-M. Binding of the pY site in CD28 (pY-M-N-M) by PI3K and Grb2 through their SH2 domains is a key step that triggers the CD28 signal transduction for T cell activation and differentiation. In this study, we determined the crystal structure of the Grb2 SH2 domain in complex with a pY-containing peptide derived from CD28 at 1.35 Å resolution. The peptide was found to adopt a twisted U-type conformation, similar to, but distinct from type-I β-turn. In all previously reported crystal structures, the peptide bound to the Grb2 SH2 domains adopts a type-I β-turn conformation, except those with a proline residue at the pY+3 position. Molecular modeling also suggests that the same peptide bound to PI3K might adopt a very different conformation.

Citation: Higo K, Ikura T, Oda M, Morii H, Takahashi J, et al. (2013) High Resolution Crystal Structure of the Grb2 SH2 Domain with a Phosphopeptide Derived from CD28. PLoS ONE 8(9): e74482. doi:10.1371/journal.pone.0074482

Editor: Jon C.D. Houtman, University of Iowa, United States of America

Received May 30, 2013; **Accepted** August 1, 2013; **Published** September 30, 2013

Funding: This work was in part supported by JSPS KAKENHI Grant Number 20159453 (http://www.jsps.go.jp/english/). The funders had no role in study design, data collection and analysis, decision to publish, or preparation of the manuscript.

Competing Interests: The authors have declared that no competing interests exist.

* E-mail: ito.str@tmd.ac.jp

Introduction

Src homology 2 (SH2) domains are critical components of intracellular proteins that promote signal transduction. SH2 domains recognize phosphotyrosine (pY)-containing sequences in proteins. Growth-factor receptor-bound protein 2 (Grb2) is an adaptor protein that has an SH3-SH2-SH3 domain architecture [1]. The Grb2 SH2 domain mediates activation of the Ras pathway through binding to phosphotyrosyl motifs on either growth factor receptors such as epidermal growth factor receptor or other adaptor proteins such as Shc [2]. Grb2 SH2 specifically binds to the pY-X-N-X consensus sequence where X is any amino acid; however, it binds to pY-(L/V)-N-(V/P) with higher affinity [3,4]. The selective inhibition of Grb2 SH2 binding to phosphorylated proteins is expected to be useful for the prevention of hyperproliferative diseases.

Three-dimensional structures of Grb2 SH2 in complex with peptides containing pY determined at atomic resolution can be useful for inhibitor development, and several such structures have been reported [4–7]. These studies showed that peptides bound to Grb2 SH2 typically adopt a type-I β-turn conformation.

Ligand binding to the CD28 receptor on the T cell surface is a costimulatory signal that acts, along with recognition of the antigen-major histocompatibility complex by the T cell receptor, to trigger full T cell activation and differentiation into effector T cells [8]. A number of signaling molecules such as Grb2 and phosphatidylinositol 3-kinase (PI3K) bind to the cytoplasmic region of CD28 and activate CD28-mediated costimulatory signaling [9,10]. These molecules bind to CD28 via their SH2 domains primarily to the sequence pY-M-N-M. The consensus Grb2 SH2-binding sequence is pY-X-N-X, whereas the PI3K SH2-binding consensus sequence is pY-X-X-M. CD28 contains the sequence pY-M-N-M in its cytoplasmic region, which enables it to bind both Grb2 SH2 and PI3K SH2 [9]. However, little is known about the molecular details of these interactions.

In this study, we report the crystal structure of Grb2 SH2 in complex with a CD28-derived peptide consisting of 8 amino acids, including the pY-M-N-M sequence, at a resolution of 1.35 Å. This is the first report of the structure of CD28 bound to Grb2 SH2. The high-resolution structure revealed that the bound peptide adopts a conformation similar to, but distinct from the canonical type-I β-turn. Such deviations might exist in other Grb2 SH2/peptide complexes. The possibility that this same peptide adopts a very different conformation when bound to PI3K SH2 is also discussed.

Materials and Methods

Expression and purification of the Grb2 SH2 domain

The SH2 domain of human Grb2 (residues 60–152) was expressed in *Escherichia coli* Bl21(DE3) cells as a glutathione *S*-transferase (GST)-fusion protein using the pGEX-4T-1 vector (GE Healthcare) in LB medium containing 100 μg/mL ampicillin. Protein expression was induced with 0.1 mM isopropyl β-D-1-

Table 1. Statistics for data collection and structure refinement.

Data collection	
Spacegroup	$P6_122$
Unit cell parameters	
a, b, c (Å)	59.0, 59.0, 117.1
Resolution (Å)	50–1.35 (1.37–1.35) *
R_{sym}	0.057 (0.498)
Completeness (%)	97.7 (98.4)
Redundancy	20.6 (21.2)
Refinement	
Resolution (Å)	50–1.35
Number of reflections	26430
R_{work}/R_{free}	0.176/0.209
Number of non-hydrogen atoms	938
(Protein atoms)	869
(Ion atoms)	5
(Water atoms)	64
RMS deviations from ideal values	
Bond length (Å)	0.020
Bond angles (degree)	2.106
Average B-factor of protein atoms (Å^2)	19.0

*Values shown in parentheses are for the highest-resolution shell.
doi:10.1371/journal.pone.0074482.t001

thiogalactopyranoside (IPTG) at 20°C, and the culture was grown for 12 hours. For Grb2 SH2 protein purification, the *E. coli* cell pellet was suspended in lysis buffer (50 mM Tris HCl [pH 8.0] and 150 mM NaCl) and sonicated on ice. After centrifugation, the supernatant was applied to glutathione sepharose 4B beads (GE Healthcare) and eluted with elution buffer (20 mM Tris HCl [pH 8.0], 200 mM NaCl, 500 µM dithiothreitol (DTT), and 10 mM reduced glutathione). The GST protein was separated from Grb2 SH2 by proteolytic cleavage with thrombin (at room temperature, overnight). The Grb2 SH2 protein was further purified by anion-exchange chromatography with a NaCl gradient (0–1.0 M NaCl in 20 mM Tris HCl [pH 8.0]) and gel-filtration chromatography at 4°C. Finally, the purified Grb2 SH2 protein was concentrated to 5 mg/mL in 20 mM Tris HCl (pH 8.0) and 100 mM NaCl.

Synthesis of the CD28-derived peptide

The 8-residue phosphopeptide, S-D-pY-M-N-M-T-P, which corresponds to residues 189–196 of human CD28, was synthesized by the Fmoc solid-phase method with a PSSM8 peptide synthesizer (Shimadzu Corp.). The C-terminus is a carboxyamide group prepared with Fmoc-NH-SAL-PEG resin (Watanabe Chemicals). Phosphorylated tyrosine was incorporated at the specific position by using *O*-monobenzyl-protected Fmoc-phosphotyrosine (Fmoc-Tyr(PO(OBzl)OH)-OH) [11]. After completion of chain-elongation, the products were cleaved using a mixture of trifluoroacetic acid, 1,2-ethanedithiol, tri-isopropyl silane, and water (86:6:6:2). The peptides were precipitated with diethyl ether, purified by reverse-phase HPLC using YMC-Pack-Pro-C18 column (YMC Co., Ltd.), and verified by mass spectrometry (Shimadzu QP-8000α). Phosphorylation was confirmed by an 8-nm blue shift of the absorption band for tyrosine.

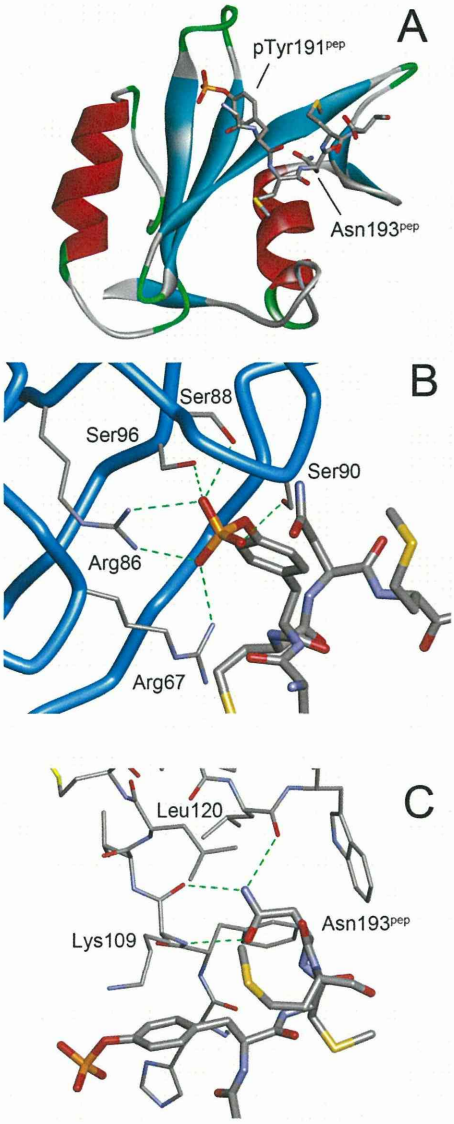

Figure 1. The structure of the Grb2 SH2 domain in complex with a CD28-derived peptide. (A) The overall structure. Grb2 SH2 is shown as a cartoon model, whereas the peptide is shown as a stick model. (B) The interactions between the phosphotyrosine, pTyr191^{pep}, and the SH2 domain. The main-chain trace of the SH2 domain is shown as blue tubes with the side-chains of some key residues in thin sticks. The phosphopeptides are shown as thick stick models. The green dashed lines indicate hydrogen bonds. (C) The interactions between the conserved asparagine, Asn193^{pep}, of the peptide (thick sticks) and the SH2 domain (thin sticks).
doi:10.1371/journal.pone.0074482.g001

Crystallization of the Grb2 SH2/CD28 peptide complex

The crystals of the Grb2 SH2/CD28 peptide complex were obtained by the hanging-drop method. Initial screening was performed with Crystal Screen and Crystal Screen 2 (Hampton Research Inc.), which produced small crystals. After refining the conditions, rod-like crystals, up to 200 µm long, were obtained in 100 mM HEPES (pH 7.5), 1.25 M sodium acetate, and 100 mM cadmium sulfate.

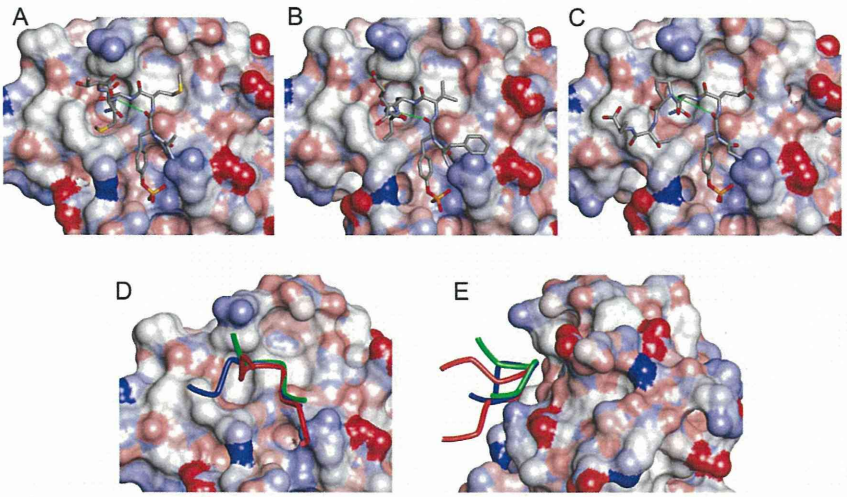

Figure 2. Comparison of the structures of phosphopeptides bound to Grb2 SH2. (A) CD28 (present work, D-pY-M-N-M-T). (B) BCR-Abl (a typical type-I β-turn, PDB ID: 1BMB, F-pY-V-N-V-E) (C) AICD (with a Pro residue at the pY+3 position, PDB ID: 3MXC, G-pY-E-N-P-T-Y). The SH2 domains are shown as surface models, whereas the phosphopeptides are shown as stick models. The thin green lines indicate the distance between the main-chain O of pY and the main-chain N of pY+3, which form a hydrogen bond in the type-I β-turn. The side-chains of some flanking residues are missing due to their weak electron density. (D) Superposition of the 3 peptides. The tubes represent the main-chain traces of CD28 (green), BCR-Abl (red), and AICD (blue). (E) Superposition of CD28, BCR-Abl, and AICD as in (D) but vertically rotated by approximately 90°.
doi:10.1371/journal.pone.0074482.g002

Data collection, structure determination, and refinement

Diffraction data was collected from a single crystal at Beamline NW12A of the Photon Factory (Tsukuba, Japan) at 100K. The diffraction data were integrated and scaled using HKL2000 (HKL Research Inc.). The space group was $P6_122$ ($a = 59.0$ Å, $b = 59.0$ Å, $c = 117.1$ Å) and the asymmetric unit contained a single Grb2 SH2/CD28 peptide complex.

Structure determination and refinement was performed using the CCP4 suite [12]. The structure was solved with PHASER [13] by molecular replacement using another previously reported Grb2 SH2 structure [14]. The structure was refined using REFMAC [15] with restrained anisotropic temperature factors. The graphics program Coot was used for model building [16]. In the last cycle of the refinement, the positional restraints for the phosphotyrosine side-chain were removed to allow the diffraction data to determine its structure. The figures were prepared using Discovery Studio (Accelrys Inc.) and Molscript [17].

Some statistics for data collection and structure refinement are shown in Table 1. The coordinates and structural data for the complex have been deposited in the Protein Data Bank (PDB ID: 3WA4).

Table 2. Main-chain torsion angles (φ/ψ) of the phosphopeptide bound to the Grb2 SH2 domain and their amino acid sequences[a].

PDB ID	Resolution (Å)	pY+1	pY+2 [N]	pY+3	O–N distance[b] (Å)
1BMB	1.8	−52.9/−33.4 [V]	−99.6/14.2	[V]	3.03
1BM2	2.1	−58.9/−44.5 [V]	−83.0/−12.6	[V]	3.22
1JYR	1.55	−59.0/−32.3 [V]	−103.8/14.9	[V]	3.11
1TZE	2.1	−54.9/−28.9 [V]	−103.2/12.8	[V]	3.02
1ZFP	1.8	−61.8/−43.4 [I]	−88.0/19.8	[Q]	3.37
3N8M	2.0	−52.4/−35.0 [V]	−100.7/10.9	[V]	3.07
CD28[c]	1.35	−72.7/−21.5 [M]	−103.6/39.8	[M]	3.71
β-turn[d]	–	−60/−30	−90/0	–	–
3MXC	2.0	−67.3/−32.9 [E]	−99.2/127.0	[P]	5.10
3MXY	2.3	−60.6/−40.3 [V]	−92.8/142.8	[P]	5.11

[a]The angles are given in degree. The residues in the pY+1 and pY+3 positions are shown as one-letter codes in square brackets.
[b]The distance between the main-chain O of pY and the main-chain N of pY+3, which form a hydrogen bond in type-I β-turn.
[c]The structure reported in this work.
[d]Theoretically idealized values for type-I β-turn.
doi:10.1371/journal.pone.0074482.t002

Results

In general, the folds of the Grb2 SH2 domain were essentially the same as those previously reported; consisting of a central, antiparallel β-sheet flanked by 2 α-helices (Fig. 1A) [4–7]. The conformation of Trp121 of Grb2 SH2 was the same as other peptide-bound structures with a χ_1 rotation of approximately 120° compared to the peptide-free structure [7]. The phosphorylated CD28 peptide binds to the Grb2 SH2 recognition site across the exposed edge of the central β-sheet. The phosphotyrosine is located between the β-sheet and the amino-terminal α-helix, and is recognized by a number of residues (Fig. 1B&C). The phosphate moiety of the phosphotyrosine (pTyr191^{pep}, the amino acid residues of the CD28-derived peptide are denoted with a "pep" suffix hereafter) directly interacts with the side chains of Arg67, Arg86, Ser88, Ser90, and Ser96. The side-chain of Asn193^{pep} at the pY+2 position forms a pair of hydrogen bonds with the main-chain amide and carbonyl groups of Lys109. Another hydrogen bond is observed between $N_{\delta 2}$ of Asn193^{pep} and the main-chain O of Leu120. These interactions involving the conserved pTyr and Asn have also been observed in other Grb2/peptide complexes [4–7].

The 2 methionine residues, which are unique to the CD28-derived peptide, appear to contribute to the binding mainly through hydrophobic interactions. The side chain of Met192^{pep}, at

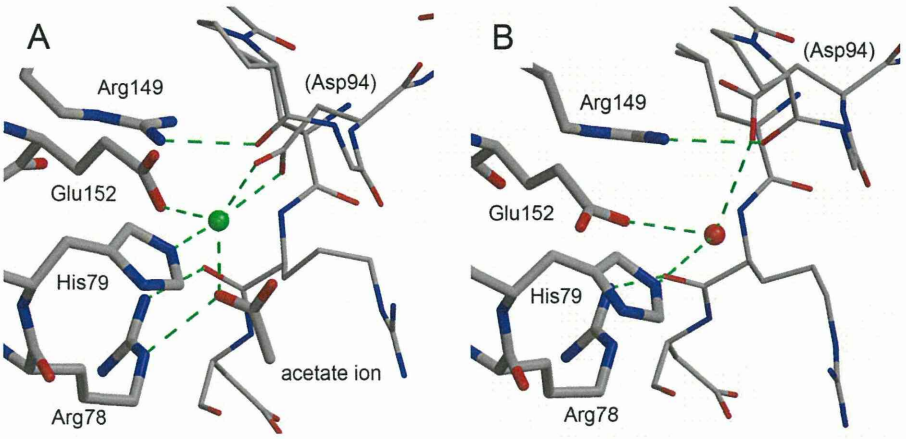

Figure 3. The cadmium binding site. (A) The cadmium binding site located between 2 neighboring molecules in the crystal. The cadmium ion is shown as a green sphere. The Grb2 SH2 molecule is shown in thick lines, whereas a symmetrically-related molecule is shown in thin lines. Green dashed lines indicated the coordinate and hydrogen bonds. (B) The corresponding site in Grb2 SH2/AICD (PDB ID: 3MXC). The red sphere represents a water molecule.
doi:10.1371/journal.pone.0074482.g003

the pY+1 position, is close to the benzene ring of Phe108 and the alkyl of Gln106. The side chain of Met194^{pep}, at the pY+3 position, interacts with Leu111 and Lys109 as well as the phosphotyrosine, although these interactions seem weaker than those of Met192^{pep} as suggested by their higher temperature factors (the average temperature factors of the side chain atoms are 27.0 Å^2 and 38.6 Å^2 for Met192^{pep} and Met194^{pep}, respectively).

The peptide adopts a bent conformation similar to the type-I β-turn, which is the canonical conformation of peptides bound to Grb2 SH2 [5,18,19]. However, the hallmark hydrogen bond between the main-chain oxygen of pY and the main-chain nitrogen of the pY+3 residue (Met194^{pep} in our structure) is not formed (Fig. 2A). Not only are they separated by greater than 3.7 Å, but the direction of the N-H bond, assuming an ordinary structure for the amide group, does not point toward the carbonyl oxygen, making the presence of the hydrogen bond unlikely. Comparison of the main-chain torsion angles φ and ψ shows that the difference between this structure and the type-I β-turn is mainly caused by the ψ angle of the conserved Asn residue at pY+2 (Table 2). In type-I β-turns, this angle should be close to 0°; however, in our structure, it is approximately 40°. Consequently, the CD28-derived peptide is slightly lifted away from Grb2 SH2, making it a more "twisted" conformation than a canonical type-I β-turn (Fig. 2D). This twist also creates more space between the peptide and the protein, and accommodates the side chain of Met194^{pep}.

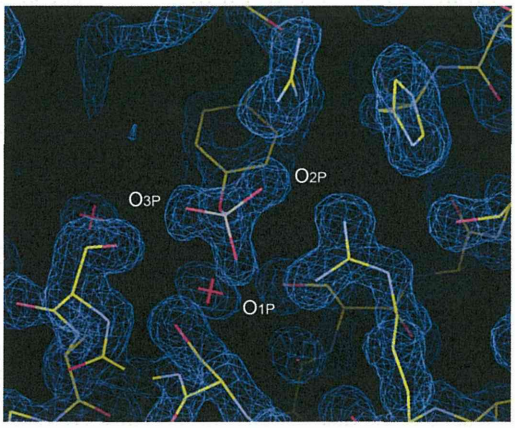

Figure 4. The 2Fo–Fc map around the phosphate group of the phosphotyrosine residue, pTyr191^{pep}. The contour level is set to 1.2 σ, where σ is the root-mean-square deviation of the electron density.
doi:10.1371/journal.pone.0074482.g004

A very strong electron density, which was interpreted as a cadmium ion, was observed between 2 molecules in the crystal lattice. This ion is coordinated by the Nε$_2$ of His79 and a carboxyl oxygen of Glu152 of one Grb2 molecule and 2 carboxyl oxygens of Asp94 in a neighboring molecule. An acetate ion, which was required for the crystallization, also coordinated to it (Fig. 3A).

In our crystallization trials, the addition of cadmium sulfate markedly improved the appearance and diffraction quality of the crystals. Among the previously reported Grb2 SH2 crystal structures, 2 (PDB ID: 3MXC and 3MXY) have the same space groups and similar unit cell parameters as our structure [20]. These 2 structures are Grb2 SH2/amyloid precursor intracellular C-terminal domain (AICD)-derived peptide structures. A comparison of these Grb2 SH2/AICD structures with ours revealed that their crystal packing is very similar. Yet the resolutions of the Grb2 SH2/AICD 2 structures, 2.0 Å and 2.3 Å, are much lower than that of our structure at 1.35 Å. In these other structures, the cadmium binding site is occupied by a water molecule that forms some hydrogen bonds (Fig. 3B). The presence of the cadmium ion appears to have increased the number of polar interactions between the 2 molecules. It may also have contributed to the improved crystal quality by replacing the intermolecular network of hydrogen bonds with stronger coordinate bonds.

The high resolution of the structure presented here allowed us to determine the geometry of the phosphotyrosine in detail (Fig. 4 & Table 3). In the very last cycle of the structure refinement, the positional constraints for the side-chain atoms of the phosphotyrosine were removed to make the most of the experimental data and investigate its geometry. Two of the three bond angles between the phenol oxygen atom and the phosphate oxygen atoms (O_η–P–O_{nP}, where n = 1, 2, or 3) are smaller than 109.5°, the

Table 3. Selected bond angles and torsion angles of the phosphate group of the phosphotyrosine (degrees).

	CD28 [a]	Small molecule crystallography [b]		REFMAC [c]
		A	B	
Bond angles				
C_ζ–O_η–P	129.6	125.5	122.8	120.0
O_η–P–O_{1P}	94.7	103.2	108.3	108.2
O_η–P–O_{2P}	106.4	104.5	106.8	108.2
O_η–P–O_{3P}	110.8	106.9	103.7	108.2
(Average of O_η–P–O_{nP})	(104.0)	(104.9)	(106.3)	(108.2)
O_{1P}–P–O_{2P}	112.9	106.5	111.0	119.9
O_{2P}–P–O_{3P}	115.6	121.5	111.4	119.9
O_{3P}–P–O_{1P}	114.1	112.5	115.0	119.9
Torsion angles				
C_ζ–O_η–P–O_{1P}	−149.0	−85.4	61.2	–
C_ζ–O_η–P–O_{2P}	−33.4	25.7	178.8	–
C_ζ–O_η–P–O_{3P}	93.0	155.6	−58.5	–
(Rotation $O_{1P} \rightarrow O_{2P}$)	(115.6)	(111.1)	(117.6)	(120.0)
(Rotation $O_{2P} \rightarrow O_{3P}$)	(126.4)	(129.9)	(122.7)	(120.0)
(Rotation $O_{3P} \rightarrow O_{1P}$)	(118.0)	(119.0)	(119.7)	(120.0)

[a]Present work.
[b]Results from small-molecule X-ray crystallography [21]. As the asymmetric unit contains 2 phosphotyrosine molecules, denoted A and B, the values for both are shown.
[c]Values from the dictionary files of REFMAC.
doi:10.1371/journal.pone.0074482.t003

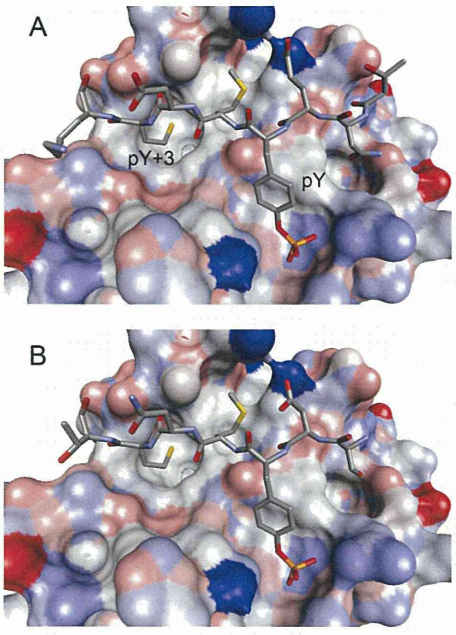

Figure 5. A model structure of the CD28-derived peptide bound to PI3K N. (A) The crystal structure of the amino-terminal SH2 domain of PI3K (PI3K N SH2) with a phosphopeptide derived from c-Kit (T-N-E-pY-M-D-M-K) and (B) a molecular model of PI3K N SH2 with the CD28-derived peptide (S-D-pY-M-N-M-T). The SH2 domains are shown as surface models, whereas the phosphopeptides are shown as stick models.
doi:10.1371/journal.pone.0074482.g005

theoretical value for ideal tetrahedral geometry, indicating that the phosphate oxygen atoms are somewhat more "spread up" than typical tetrahedral geometry. In addition, the 3 phosphate oxygens are in an asymmetrical arrangement, deviating from an equilateral triangle. To match one phosphate oxygen atom to another in a symmetrical arrangement, the rotation angle around the phenol oxygen-phosphorus bond (O_η–P) should be 120°. However, that is not the case for the phosphotyrosine in our structure. The difference between the maximum and minimum rotation angles is greater than 10°. Similar asymmetry is also observed in the phosphotyrosine molecule structures reported by small-molecule X-ray crystallography, whose resolution is 0.77 Å [21].

Discussion

Here, we reported the crystal structure of the Grb2 SH2 domain in complex with a phosphorylated peptide derived from CD28. The structure was determined at a resolution of 1.35 Å, the highest among the Grb2 SH2 domain structures reported to date. The structure revealed a unique feature of Grb2-SH2 binding to the CD28-derived peptide. In all previously reported Grb2 SH2/peptide complex structures, the peptide containing the phosphotyrosine residue adopted a type-I β-turn (Fig 2B) [19], except for the AICD-derived peptides in 2 Grb2 SH2/AICD structures [20]. The AICD-derived peptides have a proline residue at the pY+3 position and are incapable of forming a β-turn because proline does not have the amide hydrogen required for the characteristic hydrogen bond (Fig. 2C). The CD28-derived peptide reported here has a methionine residue at the pY+3 position, which is capable of forming the hydrogen bond. However, its structure is not a canonical type-I β-turn. Although it has a U-shaped conformation, similar to the β-turn, it is somewhat twisted and lacks the key hydrogen bond. This is the first such example.